Hindawi
Mathematical Problems in Engineering
Volume 2022, Article ID 5013997, 8 pages
https://doi.org/10.1155/2022/5013997

Research Article

Research on the Weak Signal Extraction Method with Adaptive Stochastic Resonance Based on the Time Grid Sensor for PMSM

Hui Wang, Fei Wang, Hongxia Liu, Yanqiu Xiao, and Guoning Shi

College of Mechanical Engineering, Zhengzhou University of Light Industry, Zhengzhou, China

Correspondence should be addressed to Fei Wang; wangfei-2015@qq.com

Received 11 February 2022; Accepted 31 March 2022; Published 26 April 2022

Academic Editor: Yu-Ling He

Because the output signal of the time grid sensor is so weak and is easily affected by the disturbing noise, it is difficult to extract the induction signal containing the position information, when the time grid sensor is used to detect the rotor position of the permanent magnet synchronous motor (PMSM). In this paper, an adaptive monostable stochastic resonance method is proposed to realize the weak signal detection of the time grid sensor. The tunnel magnetoresistance effect sensor (TMR) is adopted to detect the change of the rotor magnetic field of the motor in this method, and the detection model of the time grid sensor about PMSM is constructed. The monostable stochastic resonance theory is applied to extract the induction signal of the time grid sensor. As to the problem of the tuning the parameters of the monostable stochastic resonance system, the genetic algorithm is adopted to optimize the parameters of the monostable stochastic resonance system. The experimental results show that the monostable stochastic resonance method based on the genetic algorithm can effectively detect the weak induction signal of the time grid sensor about PMSM. This method solves the problem of the weak signal extraction of the time grid sensor for PMSM, and the detection accuracy is also improved.

1. Introduction

Permanent magnet synchronous motor (PMSM) has become very popular during the last decades due to its high efficiency, high power density, and superior dynamic response compared with other types of machines, e.g., induction or synchronous reluctance machines [1]. The commonly used position detection technology of servo motors is mainly divided into position sensor technology and sensorless technology. The former mostly relies on external sensors, such as grating, magnetic grating, and hall sensors, which severely damage the original compact structure of the motor and greatly affect its operating performance. The latter, such as back potential position estimation, model reference adaptive, high frequency signal injection, and other technologies, is greatly affected by motor parameters and has the disadvantages of low detection accuracy and complex implementation.

According to the twinness of the time grid sensor and the servo motor, the time grid is implanted into the motor structure to integrate into one, so as to realize the effective detection of the position and speed of the motor without affecting the normal driving of the motor [2]. Although this scheme can be used to achieve measurement, there are some disadvantages such as low amplitude of the induction signal and the size is easily affected by the internal and external environmental noise of the motor.

Because the internal and external operations of the servo motor are easily affected by noise, it is necessary to find a way to clearly extract the weak signal in the background of strong interference noise. In the past, signals were detected by removing and suppressing noise, such as wavelet transform and empirical mode analysis. For instance, Saadatnejad et al. proposed a new electrocardiogram (ECG) classification algorithm for continuous cardiac monitoring on wearable devices with limited processing power. In contrast to many compute-intensive deep learning-based approaches, the proposed algorithm is lightweight and therefore brings continuous monitoring with accurate LSTM-based ECG classification to wearable devices [3]. Zhou et al. proposed the morphological filter-assisted ensemble empirical mode decomposition (MF-EEMD). Compared with EEMD, MF-

EEMD significantly mitigates the mode mixing problems and achieves a higher decomposition efficiency [4].

To extract the weak signal, another signal detection method is used which uses the noise to improve the signal-to-noise ratio. This method mainly uses the stochastic resonance theory. Stochastic resonance (SR) was first presented by Italian scholar R. Benzi in the article about alternation phenomenon of glaciation and heating period of Earth [5]. The stochastic resonance model has been widely applied in the weak signal detection, which has obtained abundant research result [6–8]. Zhao et al. proposed an adaptive stochastic resonance (SR) method based on the grey wolf optimizer algorithm for fast pulsar identification [9]. Li et al. proposed a multiparameter constrained potential underdamped stochastic resonance method by studying the potential model and signal-to-noise ratio of the system. The results of various bearing failure experiments show that the method has excellent weak signal extraction ability and is suitable for early fault diagnosis [10]. Lei et al. proposed an adaptive stochastic resonance (ASR) method. The ASR method utilizes the optimization ability of ant colony algorithms and adaptively realizes the optimal stochastic resonance system matching input signals [11]. He et al. took the delayed feedback system as a model and successfully detected the target frequency and amplitude of weak signals by adjusting the model parameters, signal amplitude, and noise intensity to induce stochastic resonance [12]. Wang et al. proposed a terahertz radar signal detection method based on the adaptive stochastic resonance theory and subsampled the noise-containing difference frequency signal as well as completed the ranging calculation [13]. Cui et al. studied the stochastic resonance characteristics of the bistable circuit and conducted an experimental simulation of its circuit in the Multisim simulation environment. It is verified that the bistable circuit can achieve the stochastic resonance function very well, and it provides strong support for the actual production of the bistable circuit [14]. Huang et al. proposed an adaptive stochastic resonance (ASR) method based on GST and implemented it by quantum particle swarm optimization algorithm. Through the bearing fault simulation signal, the ASR method with the GST is compared with the normalized scale transformation (NST) stochastic resonance (SR). The results show that the efficiency of the GST method is higher than that of the NST in recognizing bearing fault feature information [15]. Qiu et al. proposed an adaptive reinforcement learning and genetic algorithm to tune the parameters of the SR system. This method combines reinforcement learning with genetic algorithm (GA), which improves the local search ability of traditional genetic algorithm, accelerates the convergence speed, and is more suitable for signal detection in UAC [16]. Lai et al. proposed a multiparameter-adjusting SR model for the standard tristable system, and its parameter adjustment rules for different input signals to produce SR are fully studied [17].

In order to realize the detection of the rotor position of PMSM, the time grid sensor is adopted to detect the change of the rotor magnetic field in this paper. The monostable stochastic resonance technology is utilized to extract the weak output signal of the time grating sensor, and the genetic algorithm is used to optimize the structure parameters of the monostable stochastic resonance system.

2. Position Detection Principle of PMSM

2.1. Operation Principle of Time Grating Sensor. The time grid sensor originally invented by Professor Donglin Peng is a displacement sensor, and it adopts the theory of "space-time coordinate transformation" (TST) [18]. The core content of the theory is "space-time coordinate conversion," that is, there is a pair of relative coordinate systems, and the displacement variable in one coordinate system is converted to the time variable in the other coordinate system to use time to measure space variable.

According to the idea of "space-time coordinate conversion," a coordinate system of uniform motion is the key to measure space with time [19]. The traveling wave can be divided into the space traveling waves and the time traveling waves by the time grating sensors. The space traveling wave travels forward and backward along the spatial displacement axis. As a typical representative of the space traveling wave, the magnetic traveling waves are often associated with the mechanical motion, and its mathematical expression can be expressed as

$$y(x,t) = A_m \sin 2\pi\left(\frac{x}{W} + \frac{t}{T}\right), \tag{1}$$

where A_m is a constant coefficient, T is the period, and W is the space pitch.

According to the calculation method of the trigonometric function, a traveling wave can be decomposed into two waves with a phase difference of 90°:

$$\begin{cases} y_1(x,t) = A_m \sin\alpha \cos\beta, \\ y_2(x,t) = A_m \cos\alpha \sin\beta, \end{cases} \tag{2}$$

where α is the time independent variable and β is the space independent variable.

The equation shows that the construction of two orthogonal wave signals is the key to the position detection of the time grating sensor.

2.2. Position Detection Principle of PMSM with Time Grid Sensors. According to the similarity between the time grid sensor and the servo motor, the rotor with the permanent magnets can be regarded as the time grating rotor, and a pair of TMR sensors placed orthogonally in space can be used as the time grating fixed probe to sense the internal rotating magnetic field of the motor to realize position detection for PMSM with the embedded time grid sensor [20, 21].

Two TMR sensors which are placed orthogonally in space are fed into two orthogonal excitation signals at the same time. The signals u can be expressed as

$$\begin{cases} u_2 = U_m \sin(\omega t), \\ u_1 = U_m \cos(\omega t), \end{cases} \tag{3}$$

where U_m is the input voltage amplitude and ω is the frequency of the excitation signal.

Because the TMR sensor can produce the linear voltage within a certain magnetic field variation range [22], the output signal is expressed as

$$V_{\text{out}} = SU_m B = KBU_m, \tag{4}$$

where V_{out} is the differential output voltage of TMR sensor, B is the sensor-induced magnetic field strength, S is the sensor sensitivity, and K is the proportional coefficient.

According to the (4), the sensor output is related to the input voltage and the external magnetic field changes. If a sinusoidal voltage, u(t), is used as the excitation signal and an external magnetic field, B(x), whose magnetic field strength changes with the spatial displacement is applied to the TMR sensor, the output of the sensor at this time is

$$V_{\text{out}} = KB(x)u(t). \tag{5}$$

According to the analysis of the above TMR sensor, the magnetic field can be detected above the permanent magnet. It can be expressed as

$$\begin{cases} B_1 = B_0 \sin \dfrac{2\pi x}{W}, \\ \\ B_2 = B_0 \cos \dfrac{2\pi x}{W}, \end{cases} \tag{6}$$

where B_0 is the magnetic induction intensity at the current position and x is the distance between the two TMR sensors.

According to (5), the two sensors' output can be expressed as

$$\begin{cases} V_1 = KB_0U_m \sin\left(\dfrac{2\pi x}{W}\right)\cos(\omega t), \\ \\ V_2 = KB_0U_m \cos\left(\dfrac{2\pi x}{W}\right)\sin(\omega t). \end{cases} \tag{7}$$

By superimposing the two signals, the traveling wave signal carrying the rotor position information can be obtained:

$$V_{\text{out}} = V_1 + V_2 = KB_0U_m \sin\left(\frac{2\pi x}{W} + \omega t\right). \tag{8}$$

2.3. Position Solution Method about the Time Grid Sensor. In order to get the rotor position of PMSM, the output signal of the time grid sensors should be calculated. The excitation signal is a reference signal, and its amplitude changes with time. The amplitude of the time grid sensor's output signal changes with the time and the spatial locations of the rotor. In addition, two signals have the same amplitude frequency. The phase difference between two signals will be obtained with the motor running. The phase difference corresponds to the time difference, ΔT. The reference signal and the traveling wave signal are shown in Figure 1. U_a is the reference signal, and U_b is the traveling wave signal.

For convenience of phase comparison, two signals could be transformed into two square wave signals. The cycle count and phase difference of two square signals will be obtained by using the high-frequency pulse interpolation technology. The square wave signals are shown in Figure 2.

The expression of displacement is obtained:

$$x = v\Delta T = \left(\frac{W}{T}\right)\Delta T, \tag{9}$$

where x is the electrical displacement and v is the speed of magnetic field rotation.

3. Weak Signal Processing Method for Time Grid Sensor

3.1. Monostable Stochastic Resonance Theory. Stochastic resonance is a phenomenon in which the output signal of the system is enhanced; this phenomenon is caused by the synergistic effect of the weak periodic signal and the noise under certain nonlinear conditions. The monostable stochastic resonance model is taken as the research object in this paper. The nonlinear equation can be expressed by the Langevin equation [23–25]:

$$X'(t) = -U'(x) + F(t) + (t), \tag{10}$$

where $F(t)$ is a periodic excitation signal, $\xi(t)$ is the Gaussian white noise, $U(x)$ is the fourth-order asymmetric potential function, and $X'(t)$ is the derivative of the system output signal.

Langevin differential equations can be solved by the following fourth-order Runge–Kutta method:

$$\begin{cases} s_n = F_n(t) + \xi_n(t), \\ \\ k_1 = h\left(ax_n - bx_n^3 + s_n\right), \\ \\ k_2 = h\left[a\left(x_n + \dfrac{k_1}{2}\right) - b\left(x_n + \dfrac{k_1}{2}\right)^3 + s_n\right], \\ \\ k_3 = h\left[a\left(x_n + \dfrac{k_2}{2}\right) - b\left(x_n + \dfrac{k_2}{2}\right)^3 + s_{n+1}\right], \\ \\ k_4 = h\left[a(x_n + k_3) - b(x_n + k_3)^3 + s_{n+1}\right], \\ \\ x_{n+1} = x_n + \dfrac{1}{6}(k_1 + 2k_2 + 2k_3 + k_4), \\ \\ n = 0, 1, \ldots, N-1, \end{cases} \tag{11}$$

where N is the number of the input data, x_n represents the system output value at time n, k_1 is the time start slope, k_2, k_3 represent the time midpoint slope, k_4 is the time end slope,

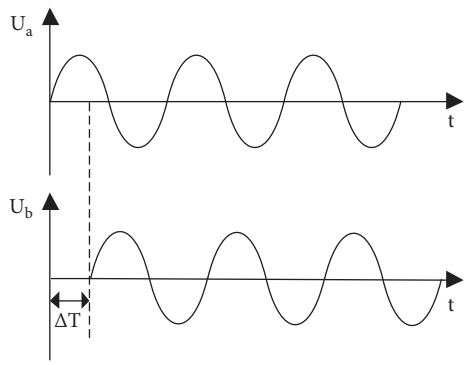

Figure 1: Reference signal and traveling wave signal with phase difference.

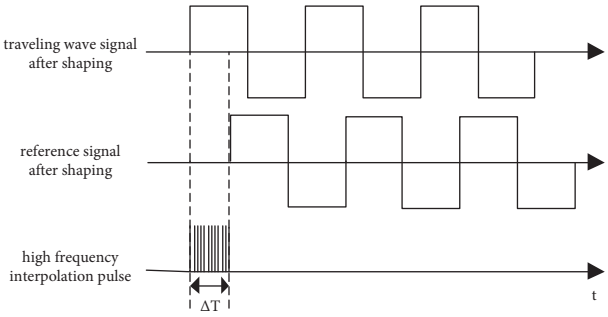

Figure 2: Square signal after shaping.

that is, the differential at a point, and h is the integration time step.

The derivative expression of the potential function $U(x)$ of a typical overdamped monostable system can be expressed as

$$U'(x) = ax^3 - b, \tag{12}$$

where a and b are constants, which represent the asymmetry of the system and are called nonlinear coefficients.

The statistical properties of the white noise used in stochastic resonance systems should meet the following requirements:

$$\begin{cases} (t) = 0, \\ (t)(s) = 2\ D\delta(t-s), \end{cases} \tag{13}$$

where $\langle\cdot\rangle$ is the overall average operator, $\xi(s)$ is the initial condition of the SR system, and D is the noise intensity.

Assuming that $\mathrm{P}(x,t)$ is the probability distribution function of the SR variable x and C is constant, using its expansion and statistical properties of white Gaussian noise, the corresponding Fokker–Planck equation can be obtained:

$$\frac{\partial \mathrm{P}(x,t)}{\partial t} = \left[-\frac{\partial G(x)}{\partial x} + \frac{\partial^2 H(x)}{\partial x^2}\right]\mathrm{P}(x,t). \tag{14}$$

Among them, the expression of $G(x)$, $H(x)$ is as follows:

$$\begin{cases} G(x) = Dx - U'(x) + F(t), \\ H(x) = Dx^2 + C. \end{cases} \tag{15}$$

If the signal amplitude and frequency is far smaller than one, that is, $f \ll 1$, the system can be considered to achieve a local equilibrium within an excitation period. The adiabatic approximation condition is satisfied.

According to Fokker–Planck equation (14), the quasi-steady-state distribution function of the system is

$$Q_{st}(x) = \frac{M_{st}}{\sqrt{H(x)}\cdot e^{E(x)/D}}, \tag{16}$$

where M_{st} is a normalized constant and $E(x)$ is the generalized potential function.

$E(x)$ can be expressed as

$$E(x) = D\int_{-\infty}^{x} \frac{Dx - U'(x) + F(t)}{Dx^2 + C}dx\ . \tag{17}$$

Because the equivalent potential function $E(x)$ has a similar form with the potential function $U(x)$ of the bistable system, the monostable system can be regarded as the equivalent bistable system when $D \neq 0$, and the transient state and the steady state can be, respectively, expressed as $x_0 = 0$ and $x_{\mp} = \mp\sqrt{D/a}$.

When the monostable system parameters, the signal, and the noise are matched, the periodic weak signal can be properly enhanced. Therefore, seeking an appropriate parameter adjustment stochastic resonance algorithm plays a key role in improving the detection adaptability.

3.2. Parameter Optimization Method of the Monostable Stochastic Resonance System. As to the problem of tuning parameter about the traditionally monostable stochastic resonance algorithm, the extraction of the position information is not very effective. In this paper, the genetic algorithm is applied to the monostable stochastic resonance system to determine the value of parameters a and b to optimize the parameters.

The specific steps for optimizing the system parameters with the genetic algorithm are as follows.

Step 1. Coding: set the respective search range and precision of the stochastic resonance system parameters. Then, calculate the corresponding code length to obtain the individual code in the group, $e_m e_{m-1} e_{m-2} \cdots e_1 f_n f_{n-1} f_{n-2} \cdots f_1$.The formula used for parameter binary encoding is

$$\begin{cases} 2^c - 1 = \dfrac{(l_{\max} - l_{\min})}{\delta}, \\ 2^{\,d} - 1 = \dfrac{(k_{\max} - k_{\min})}{\delta}, \end{cases} \tag{18}$$

where c and d are the coding lengths of the two parameters, $[l_{\min}, l_{\max}]$, $[k_{\min}, k_{\max}]$ represent the corresponding search range, and δ is the precision.

Step 2. Initializing the population: according to the population number, the individual is randomly selected to initialize the population.

Step 3. Decoding: according to the following individual decoding equation, the stochastic resonance system parameters a and b are obtained.

$$\begin{cases} a = l_{\min} + \left(\sum_{i=1}^{m} e_i 2^c - 1 \right) \dfrac{l_{\max} - l_{\min}}{2^m - 1}, \\ b = k_{\min} + \left(\sum_{j=1}^{n} f_j 2^{\ d} - 1 \right) \dfrac{k_{\max} - k_{\min}}{2^n - 1}. \end{cases} \tag{19}$$

Step 4. Building fitness function: the system output signal-to-noise ratio (SNR) is used as the fitness index function. Calculate the fitness value of the individual. The SNR expression of the output signal is

$$SNR = 20lg \frac{|X(k_0)|}{\sum_{k=0}^{N-1} |X(k)| - 2|X(k_0)|}, \tag{20}$$

where $X(k)$ is the Fourier transform of the stochastic resonance system output signal at time k.

Step 5. Choosing crossover and mutation: according to the adaptable fitness function, the excellent individuals based on crossover and mutation are selected to reconstitute a new generated population.

Step 6. Terminating: the above generated population process is repeated until that the set number of iterations is met. The optimized structural parameters of the stochastic resonance system are obtained at this time.

In order to verify the validity of the above method, the simulation experiment is conducted. The effective input signal is $F(t) = 0.5 \cos(10\pi t)$, the system noise input signal is $\Gamma(t) = \sqrt{2D}\xi(t)$, $\xi(t)$ is the Gaussian white noise with mean 0 and variance 1, and D is the noise intensity. Then, the mixed signal is $S(t) = F(t) + \Gamma(t)$. The initial population $M = 300$, evolutionary algebra NG = 100, the search range of a parameter is a $\in$ (0.01~20), the search range of b parameter is b$\in$ (0.01~10̄5), the crossover probability $P_c = 0.93$, and the mutation probability $P_m = 0.02$. When the population converges, the optimal stochastic resonance state is reached. The simulation results are shown in Figures 3–6.

Figure 3 shows the mixed input signal waveform. Figure 5 shows the output signal waveform. After stochastic resonance algorithm processing, the useful signal components are preserved, the image is clear, and the outline is obvious. Figure 4 shows the mixed input signal spectrum. Figure 6 shows the output signal spectrum. Comparing Figure 4 with Figure 6, the above simulation shows that the noise interference is reduced, and the system is in a state of random resonance. A clear peak can be clearly observed. The corresponding frequency is about 5 Hz, which is equal to the measured weak signal frequency.

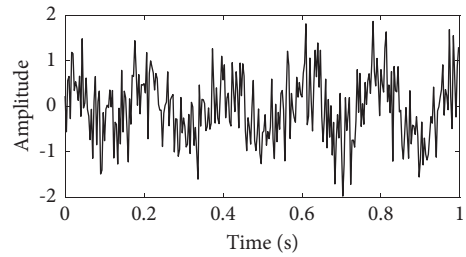

Figure 3: Input signal S(t).

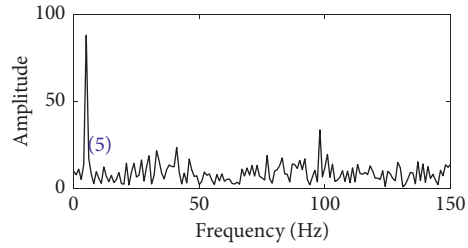

Figure 4: Input signal spectrum.

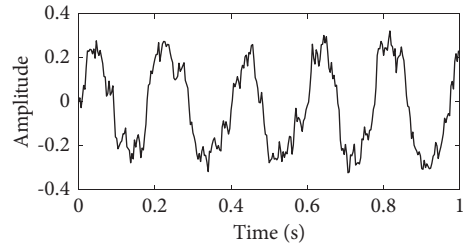

Figure 5: Output signal X(t).

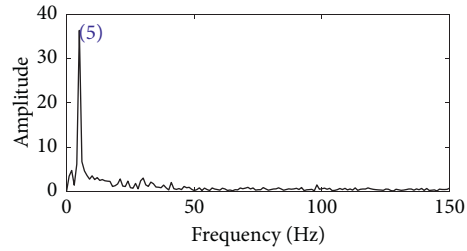

Figure 6: Output signal spectrum.

4. Experimental Analysis

In order to prove the validity of the embedded position detection system based on the time grid sensor about PMSM, an experiment platform is set up as shown in Figure 7.

This platform mainly includes PMSM (model: 80ST-MO1330) with the time grid sensor, a control board with the master chip of TMS320F28335, a motor drive board (model: IPMV3A3), and a signal processing board. The main parameters of the PMSM are shown in Table 1.

The installation position of the two TMR chip is shown in Figure 8. A pair of TMR chips with the difference of 67.5° is fixed on the round PCB. The PCB and the motor rear cover

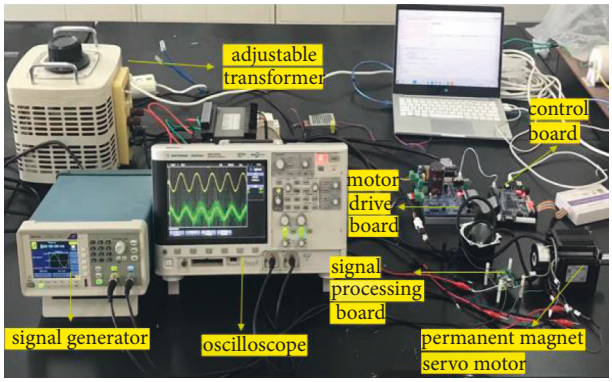

Figure 7: Embedded signal detection system.

Table 1: PMSM parameters used.

Parameter	Value	Unit
Rated line voltage	220	V
Rated line current	2	A
Rated torque	1.27	N.m
Pole number	8	Pole
Rotor inertia	$1.05 \bullet 10^{-4}$	$kg \bullet m^2$
Winding resistance	4.44	Ω
Winding inductance	7.93	mH
Electrical constant	1.66	ms
Encoder line number	2500	PPR

are fixed together. According to the embedded measurement principle, the time grating sensor will sense a pair of traveling wave signals containing angular displacement after the motor is started.

After connecting and powering up in the above manner and running DSP to control PMSM speed at a uniform rotate of 60 rpm, the used oscilloscope will obtain the two induced traveling wave signals and the voltage amplitude is amplified about 2 V, as shown in Figure 9.

According to the above signal extraction method of time grid sensor based on adaptive stochastic resonance theory, two induced traveling wave signals are superimposed to obtain an angular displacement signal, as shown in Figure 10.

To clearly analyze the characteristics of the angular displacement signal, Figure 10 is again enlarged within 0.2 s. From Figure 10 or 11, the angular displacement is a sinusoidal waveform with phase shift, small amplitude changes, and harmonic interference. To remove the influence of noise on the induction signal of the time grid sensor, adaptive stochastic resonance processing is performed on the superimposed traveling wave signal.

In the genetic algorithm model, the signal sampling frequency fs = 70100 Hz. Figure 12 shows the input signal spectrum. There are obvious peaks in the output signal spectrum (Figure 13), its amplitude is 0.14477 at the frequency of 1 kHz, and the tested signal is successfully detected.

The corresponding adaptive stochastic resonance output waveform is shown in Figure 14. The partial amplification of output signal has a clear waveform without obvious harmonic interference within 0.2 s as shown in Figure 15. Comparing the output graph with inputting signal, original signal waveform including noise is significantly reduced, and the useful components of the signal are retained.

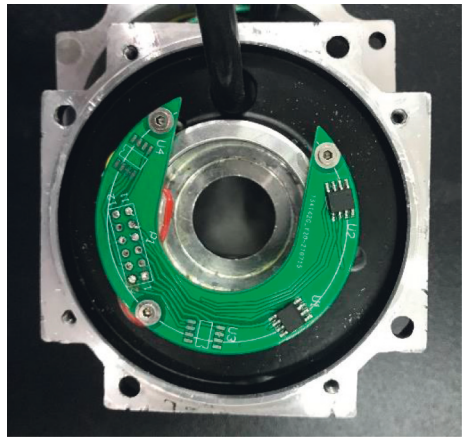

Figure 8: Chip mounting position.

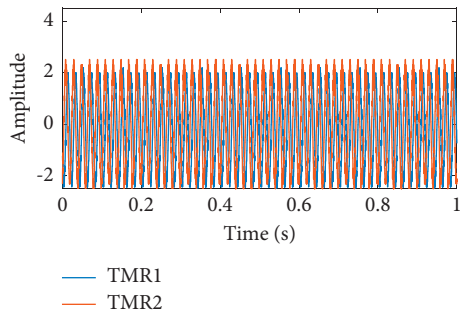

Figure 9: Traveling wave signal.

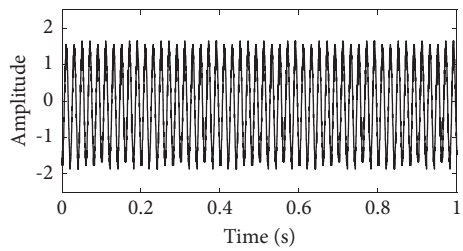

Figure 10: Angular displacement signal.

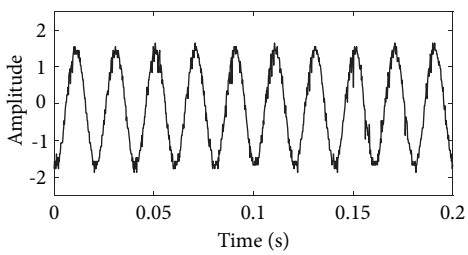

Figure 11: Partial amplification of the displacement signal.

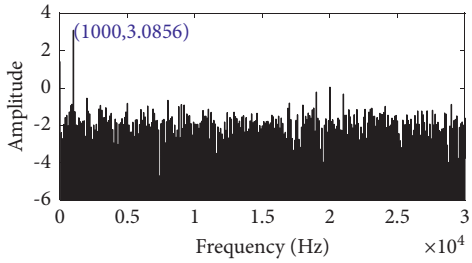

Figure 12: Input signal spectrum.

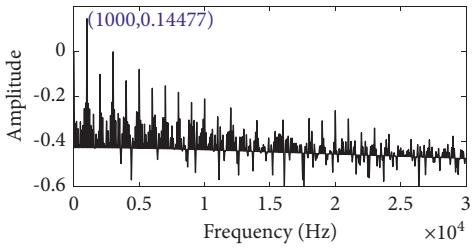

Figure 13: Output signal spectrum.

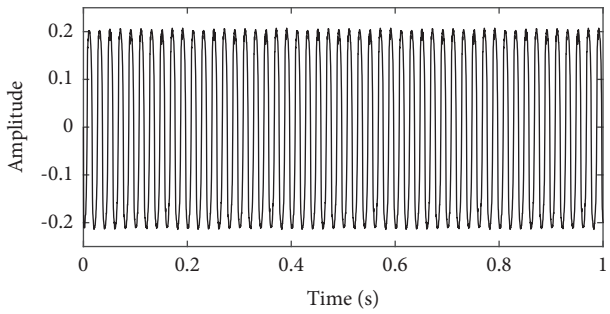

Figure 14: SR system output signal.

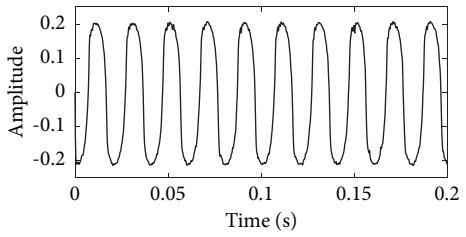

Figure 15: Partial amplification of the output signal.

The induced signal is shaped into a square wave signal as shown in Figure 16. The vertical axis is zero to one in the cycle.

Phase difference is interpolated by high-frequency pulse technology between adaptive stochastic resonance output signal and reference signal to obtain the PMSM rotational angular displacement as shown in Figure 17. The unit of motor running time is seconds, and the slope of the curve should represent the speed, which is basically the same as the set speed of the servo motor. The results show that this method can realize the rotor position detection of the synchronous motor.

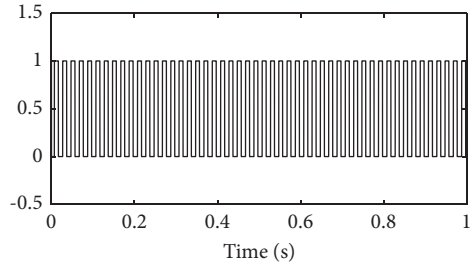

Figure 16: Corresponding square wave.

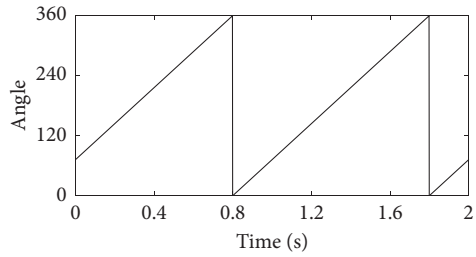

Figure 17: Angular displacement.

5. Conclusion

In this paper, the adaptive monostable stochastic resonance is proposed to extract the weak induced signal of the time grid sensor about PMSM. This method adopts the genetic algorithm to optimize the parameters of the monostable stochastic resonance system and achieves the real-time adjustment of the parameters. The position detection method based on the time grid sensor for PMSM reduces system's size of the servo motor and increases the reliability. This method also improves the position detection accuracy of PMSM.

Data Availability

The underlying data supporting the results of the study can be obtained from the corresponding author upon request.

Conflicts of Interest

The authors declare that there are no conflicts of interest regarding the publication of this article.

Acknowledgments

This study was supported by the Technological Project of Henan Province (grant no. 202102210284).

References

[1] D. Reigosa, D. Fernandez, and C. Gonzalez, "Permanent magnet synchronous machine drive control using analog hall-effect Sensors," *IEEE Transactions on Industry Applications*, vol. 54, no. 3, pp. 2358–2369, 2018.

[2] S. Wang, Z. Wu, D. Peng, and W. Li, "Research on the novel AC servo motor with position detection function," *Proceedings of the CSEE*, vol. 38, no. 22, pp. 6692–6700, 2018.

[3] S. Saadatnejad, M. Oveisi, and M. Hashemi, "LSTM-based ECG classification for continuous monitoring on personal wearable devices," *IEEE Journal of Biomedical and Health Informatics*, vol. 24, no. 2, pp. 515–523, 2020.

[4] X. Zhou, D. Shan, and Q. Li, "Morphological filter-assisted ensemble empirical mode decomposition," *Mathematical Problems in Engineering*, vol. 2018, Article ID 5976589, 12 pages, 2018.

[5] R. Benzi, A. Sutera, and A. Vulpiani, "The mechanism of stochastic resonance," *Journal of Physics A: Mathematical and General*, vol. 14, no. 5, pp. 453–457, 1981.

[6] B. Li, R. Tong, J. Kang, and K. Chi, "Bearing fault diagnosis using synthetic quantitative index-based adaptive underdamped stochastic resonance," *Mathematical Problems in Engineering*, vol. 2021, Article ID 8888079, 10 pages, 2021.

[7] Z. Li, S. Han, and J. Wang, "Time-delayed feedback tristable stochastic resonance weak fault diagnosis method and its application," *Shock and Vibration*, vol. 2019, Article ID 2097164, 13 pages, 2019.

[8] G. Zhang and H. Li, "Hybrid tri-stable stochastic resonance system used for fault signal detection," *Journal of Vibration and Shock*, vol. 38, no. 18, pp. 9–17, 2019.

[9] H. Zhao, J. Jin, B. Shan, Y. Jiang, and Y. Shen, "Pulsar identification method based on adaptive grey wolf optimization algorithm in X-ray pulsar-based navigations," *Advances in Space Research*, vol. 69, no. 2, pp. 1220–1235, 2022.

[10] Z. Li, X. Liu, X. Wang, and T. He, "A multi-parameter constrained potential underdamped stochastic resonance method and its application for weak fault diagnosis," *Journal of Sound and Vibration*, vol. 54, no. 3, Article ID 114862, 2019.

[11] Y. Lei, D. Han, J. Lin, and Z. He, "Planetary gearbox fault diagnosis using an adaptive stochastic resonance method," *Mechanical Systems and Signal Processing*, vol. 38, no. 1, pp. 113–124, 2013.

[12] L. He, Y. Yang, and T. Zhang, "Stochastic resonance characteristics of EVG system with time-delay feedback and bearing fault diagnosis," *Chinese Journal of Scientific Instrument*, vol. 40, no. 8, pp. 47–57, 2019.

[13] S. Wang and F. Wang, "Terahertz radar signal detection method based on adaptive stochastic resonance theory," *Acta Physica Sinica*, vol. 67, no. 16, pp. 5021–5027, 2018.

[14] L. Cui, J. Yang, L. Wang, and H. Liu, "Theory and application of weak signal detection based on stochastic resonance mechanism," *Mathematical Problems in Engineering*, vol. 2021, Article ID 5553490, 9 pages, 2021.

[15] D. Huang, J. Yang, and J. Zhang, "An improved adaptive stochastic resonance method for improving the efficiency of bearing faults diagnosis," *Journal of Mechanical Engineering Science*, vol. 232, no. 13, pp. 2352–2368, 2017.

[16] Y. Qiu, F. Yuan, S. Ji, and E. Cheng, "Stochastic resonance with reinforcement learning for underwater acoustic communication signal," *Nonlinear Dynamics*, vol. 2020, Article ID 5553490, 14 pages, 2020.

[17] Z. Lai, J. Liu, H. Zhang, C. L. Zhang, and J. W. Zhang, "Multi-parameter-adjusting stochastic resonance in a standard tristable system and its application in incipient fault diagnosis," *Nonlinear Dynamics*, vol. 96, no. 3, pp. 2069–2085, 2019.

[18] D. Peng and C. Liu, "Theory of time-space coordinate transform and study on time-grating displacement sensor," *Chinese Journal of Scientific Instrument*, vol. 21, no. 3, pp. 338–342, 2000.

[19] M. Fu, C. Li, G. Zhu, H. Shi, and F. Chen, "A high precision time grating displacement sensor based on temporal and spatial modulation of light-field," *Sensors*, vol. 20, no. 3, 16 pages, Article ID s20030921, 2020.

[20] W. Wang, Z. Shi, and D. Peng, "Research on compensation algorithm of time-grating sensor using d-q transformation," *Chinese Journal of Scientific Instrument*, vol. 38, no. 10, pp. 2453–2460, 2017.

[21] Z. Chen, X. Liu, K. Peng, and Z. Yu, "A self-adaptive interpolation method for sinusoidal sensors," *IEEE Transactions on Instrumentation and Measurement*, vol. 69, no. 10, pp. 7675–7682, 2020.

[22] B. Negulescu, D. Lacour, F. Montaigne, A. Gerkenb, and J. Paulb, "Wide range and tunable linear TMR sensor using two exchange pinned electrodes," *Applied Physics Letters*, vol. 9, no. 11, pp. 1–3, 2009.

[23] K. Gao, X. Xu, J. Li, S. Jiao, and N. Shi, "Research on feature enhancement method of weak fault signal of rotating machinery based on adaptive stochastic resonance," *Journal of Mechanical Science and Technology*, vol. 36, no. 2, pp. 553–563, 2022.

[24] Z. Qiao, Y. Lei, and N. Li, "Applications of stochastic resonance to machinery fault detection: a review and tutorial," *Mechanical Systems and Signal Processing*, vol. 122, pp. 502–536, 2019.

[25] H. Wang and F. Wang, "Research on adaptive detection method of shock signal based on monostable stochastic resonance," *Mechanical and Electrical Engineering*, vol. 36, no. 9, pp. 913–917, 2019.